

# Structural investigations on electrodes - electrolytes systems for intermediate temperature solid oxide fuel cell applications

L. DUTA<sup>\*</sup>, G. DORCIOMAN, A. C. POPESCU, I. N. MIHAILESCU, P. NITA<sup>a</sup>, I. MERCIONIU<sup>b</sup>, A. BIRSAN<sup>b</sup>, I. BIBICU<sup>b</sup>, S. CONSTANTINESCU<sup>b</sup>, N. POPESCU-POGRION<sup>b</sup>

*National Institute for Lasers, Plasma and Radiation Physics, Atomistilor Street 409, Magurele, Romania*

<sup>a</sup>*METAV-CD SA, C.A. Rosetti Street 31, Bucharest, Romania*

<sup>b</sup>*National Institute of Material Physics, Atomistilor Street 105 bis, Magurele, Romania*

We report on the synthesis of electrode layers by Pulsed Laser Deposition technique. We selected Nickel Oxide-8Yttria-Stabilized Zirconia as anode,  $\text{La}_{0.6}\text{Sr}_{0.4}\text{Co}_{0.2}\text{Fe}_{0.8}\text{O}_{3-\delta}$  perovskite material as cathode, and Yttria doped (Cerium- $\alpha$  Alumina) as electrolyte. We studied electrode structure (average grain size, porosity, and grain shape), the deposition uniformity and electrode-electrolyte interfaces. The electrodes were investigated in terms of morphology (Scanning Electron Microscopy) and composition (Energy Dispersive X-ray Spectroscopy). The initial powder and the synthesized cathodes have been investigated superficially and in bulk by Mössbauer spectroscopy, in order to detect and analyse local properties. We identified the conditions for electrode layer synthesis in respect with porosity, composition, and mean grain size.

(Received May 2, 2012; accepted October 30, 2012)

**Keywords:** Intermediate Temperature-Solid Oxide Fuel Cell, Nickel Oxide-8Yttria-Stabilized Zirconia,  $\text{La}_{0.6}\text{Sr}_{0.4}\text{Co}_{0.2}\text{Fe}_{0.8}\text{O}_{3-\delta}$ , Yttria doped (Cerium- $\alpha$  Alumina) electrolyte, Pulsed Laser Deposition, Electron Microscopy, X Ray Diffraction, Mössbauer Spectroscopy

## 1. Introduction

Solid oxide fuel cells (SOFC) are energy sources rapidly developing due to their high electrical power generation efficiency, low emissions and fuel flexibility [1]. Fuel cells consist of two electrodes (anode, cathode) and an electrolyte [2]. To be functional, SOFC electrodes should be porous whereas the electrolyte must be defect-free to avoid charge and gas leakage across the cell. The electrolyte should be a good ionic conductor, but highly resistant to electrons. In an SOFC, the electrolyte is a solid oxide that forms an  $\text{O}^{2-}$  charge carrier separating the oxidative and reductive half reactions. The main focus in the field is to reduce the operating temperature of SOFC from 700–1000 °C below 500–700 °C, to obtain the Intermediate Temperature Solid Oxide Fuel Cell (IT-SOFC). Among the electrolytes used for IT-SOFC, the most studied are those based on Ceria ( $\text{CeO}_2$ ). They are doped with Yttria ( $\text{Y}_2\text{O}_3$ ), Scandium trioxide ( $\text{Sc}_2\text{O}_3$ ),  $\text{Y}_2\text{O}_3 + \text{Sc}_2\text{O}_3$ , Gadolinia, Samaria, etc. Due to its performance, Nickel Oxide (NiO)-8Yttria-Stabilized Zirconia (YSZ) (50:50 vol) is considered to be a good anode material used in SOFC/IT-SOFC [5]. For cathodes,  $\text{La}_{0.6}\text{Sr}_{0.4}\text{Co}_{0.2}\text{Fe}_{0.8}\text{O}_{3-\delta}$  (LSCF) perovskite material is a promising candidate because it is a mixed electron-ion conductor. It reacts with electrolyte based on  $\text{Y}_2\text{O}_3:\text{CeO}_2$  [2, 6, 7]. The cathode and anode synthesis in form of layers can be achieved by many methods including pulsed laser deposition (PLD) [8, 9]. PLD insures the congruent

transfer of complex oxides from target to collector and confers a high adherence of the deposited layers to substrate [10-12]. Beckel *et al.* [13] synthesized by PLD cathode layers at 450 °C. The microstructure was composed of columnar grains. Ho-Sung Noh *et al.* [14] synthesized at 700 °C NiO-YSZ layers exhibiting a fine porous structure and good conductivity. The structure plays a crucial role in obtaining good results for the anode – electrolyte - cathode system. Starting from the powders, the structural investigations (Transmission Electron Microscopy, Scanning Electron Microscopy - SEM, and Energy Dispersive X-Ray Spectroscopy - EDS) must be performed for each step of sample preparation. The final properties are in a strong correlation with the microstructure. The electron microscopy stands for the main investigation method for the anode, electrolyte, cathode and anode – electrolyte or cathode – electrolyte interfaces.

Mössbauer spectroscopy has proven to be a nuclear  $\gamma$ -ray reliable technique able to evidence the chemical and magnetic ordering phases containing iron as constituent and dopant in the solid samples by hyperfine interactions between Mössbauer nuclide and its local vicinity (of the ligands and of the electronic surrounding). One can detect by the local hyperfine fields, valence and spin states of Mössbauer nuclide's ionic host, chemical bond, ionic polyhedral distortion magnetic ordering and phase transitions point (temperature, pressure doping level, etc [15, 16].

In the present paper, a study on the morphological properties of a new ceramic composite,  $Y_2O_3:(CeO_2-\alpha-Al_2O_3)$ , obtained by mechanical homogenization, pressing and sintering, used as solid electrolyte for IT-SOFC, is reported. NiO-8YSZ (50:50 vol) and LSCF layers were deposited by PLD onto the electrolyte's surface and the obtained structures were analysed by X-Ray Diffraction (XRD), SEM coupled with EDS, and Mössbauer techniques.

## 2. Experimental

### 2.1 Electrolyte - Sample preparation

The new reported ceramic composite, [(80 %) 10  $Y_2O_3: CeO_2$  + (20 %) (150 ppm)  $Y_2O_3: \alpha-Al_2O_3$ ], consists of (10 mol %)  $Y_2O_3: CeO_2$  (further noted by 10YDC) and (150 ppm)  $Y_2O_3: \alpha-Al_2O_3$  (further noted by 150Y:  $\alpha-Al_2O_3$ ). Fine 10YDC oxide nanopowders were prepared by co-precipitation. 150Y:  $\alpha-Al_2O_3$  was obtained by mechanical techniques starting from commercial powders (INFRAMAT, USA). The final composite (sintering bodies) was prepared by mixing (80%) 10YDC and (20 %) 150Y:  $\alpha-Al_2O_3$  nanopowders, pressing and sintering at 1500 °C for 2 hours. The sintered bodies were prepared for SEM by polishing and thermal etching (1400 °C, 1hour) in order to observe the grain boundaries and the porosity.

### 2.2 PLD experiments

PLD experiments were conducted inside a stainless steel deposition chamber using a KrF\* excimer laser source, model COMPexPro 205 ( $\lambda = 248$  nm,  $\tau_{FWHM} \approx 25$  ns), running at a repetition rate of 10 Hz (Fig. 1). The laser beam was incident on the target surface at 45 °. The targets for both electrodes were obtained by pressing (~5 MPa) and sintering (8 h at 1100 °C in air, with a heating rate of 20 °C/min and a cooling ramp of 5 °C/min). 10YDC + 150Y:  $\alpha-Al_2O_3$  electrolytes were used as deposition substrates. They were placed parallel to the targets, at 4 cm separation distance in front of them. The laser fluence onto the target surface was set at ~ 2.2 J/cm<sup>2</sup> (the corresponding pulse energy was of 460 mJ).

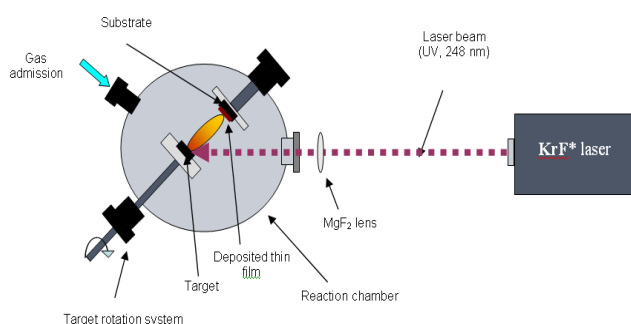


Fig. 1. PLD experimental set-up.

Before deposition, the targets were submitted to a cleaning process with 1000 laser pulses. During this procedure, a shutter was interposed between the target and the substrate to collect the flux of expelled impurities and defects. The targets were continuously rotated with 0.3 Hz and translated along two orthogonal axes to avoid piercing in order to insure a uniform deposition. The substrates were heated and maintained at a constant temperature using a PID-EXCEL temperature controller. All depositions were conducted in a dynamic oxygen flux of  $2 \times 10^{-1}$  Torr.

For the deposition of each anode layer, 35000 laser pulses were applied. The substrate temperature was maintained at a constant value of 300 °C.

The LSCF layers were deposited by 25000 subsequent laser pulses. In order to obtain crystalline compact layers, the substrate temperature was kept at 400 °C.

### 2.3 Physical-chemical investigations

#### 2.3.1 XRD

The purity of the starting material, the LSCF product and the phase structure of the final products - (LSCF/10YDC) and (LSCF//10YDC + (20 %) 150Y:  $\alpha-Al_2O_3$ ) - were examined by XRD method in a D8 ADVANCE type BRUKER-AXS diffractometer with Cu K $\alpha$  radiation ( $\lambda=1.5418\text{\AA}$ ), in the  $2\theta$  range from 15° to 140°, with a step size of 2°. The Rietveld analysis of crystal structures was carried out using a Fullprof Suite program.

#### 2.3.2 SEM and EDS

The morphology of layers deposited on [(80 %) 10YDC + (20 %) 150Y:  $\alpha-Al_2O_3$ ] substrate was investigated by SEM using a TESCAN LYRA 3 XMU and HITACHI S2600N instruments. The chemical composition of the structures was studied by EDS. The grain size and the porosity were determined by SEM images in correlation with statistical analyses.

#### 2.3.3 Mössbauer spectroscopy

For Mossbauer investigations, the LSCF layers have been deposited on standard microscope glass substrates of (76 × 26) mm<sup>2</sup>, from Hirschmann Laborgerate, under the same conditions used for the depositions onto electrolyte substrates.

Two geometries of Mössbauer techniques have used to investigate the LSCF powder and the deposited thin film. The first one is the transmission geometry (TMS), for powder, and the second one is the electron backscattering geometry (CEMS), for deposited samples. Generally, CEMS geometry is a favourable technique for thin film investigations. The electron-backscattering signal picks up and investigates up to 100Å in film's depth. In case of CEMS, the signal is given by the surface and subsurface shells, while for TMS, the signal is recorded in bulk. Therefore, the spectra of these two geometries will have

slightly different line shapes. The surface areas of the TMS and CEMS samples can be calculated with the formula  $\pi r^2$ , where  $r = 10\text{mm}$  and  $7\text{mm}$ , respectively. The LSCF spectra have been obtained at room temperature (RT), using a  $^{57}\text{Co}:\text{Rh}$  source, characterized by a nominal intensity of 50 mCi, abundance  $a_{57\text{Fe}} = 2\%$ , Mössbauer fraction  $f(\text{RT}) = 0.76$ , line-width of  $\gamma$  line-resonance  $\Gamma_{\text{exp}} = 0.22\text{ mm/s}$ , with in the energy range  $v \in [-10\text{ mm/s} \div +10\text{ mm/s}]$ , expressed in velocity units, both in  $^{57}\text{Fe}:\text{TMS}$  and CEMS. AME-20 and AME-50 PROMEDA ELSCINT/Israel spectrometers have been used. The spectra fitted by  $\chi^2$  convergence procedure has been applied to fit the spectra and extract the hyperfine parameters - chemical shift ( $\delta_{\text{A-S}}$ ), quadrupole shift ( $\epsilon_{\text{Q}}$ ), hyperfine magnetic field intensity ( $B$ ), linewidth  $\Gamma_{\text{exp}}$  and the relative absorption area of spectra ( $A$ ). The constraints of the fit model are the superposition of singlet, doublet and/or sextet patterns, with Lorentz-resonance shapes with theoretical intensities and position. The constraints of the fit model are the superposition of singlet, doublet and/or sextet patterns, with Lorentz-resonance shapes with the same line-widths, theoretical intensities and position for each of patterns.

The aim of LSCF investigation by Mössbauer technique is, on one hand, to analyse and compare the LSCF spectra of commercially nanopowders and deposited layers, in order to detect similarities and/or differences between their  $^{57}\text{Fe}$  local vicinities, and on the other hand, to evidence: (a) the magnetic ordering in samples, (b) the local crystal chemistry (Fe-O chemical bond) around nuclide and (c) the valence and spin states of ionic-host of  $^{57}\text{Fe}$ . The valence and spin states of ionic-host represent an important local property of iron mixed valence and sample conductivity.

### 3. Results and discussion

#### 3.1 Structural investigations

##### 3.1.1 Morphological characterization of electrolyte

XRD characterization at RT indicates that all studied specimens hold the LSCF phase, adopting a trigonal unit cell (space group:  $R\bar{3}c$ ) with a  $\text{La}_{0.6}\text{Sr}_{0.4}\text{Co}_{0.2}\text{Fe}_{0.8}\text{O}_{3-\delta}$  - structure. The XRD pattern of the LSCF sample can be satisfactorily reproduced by the LSCF structure with the lattice parameters  $a = 5.4877(5)\text{ \AA}$  and  $c = 13.4737(1)\text{ \AA}$  and  $\text{CeO}_2$   $a = 5.4115(5)\text{ \AA}$  (space group:  $Fm\bar{3}m$ ). The reliability indices ( $R_{\text{wp}} = 7.175\%$ ,  $R_{\text{p}} = 4.156\%$ , and  $RF = 0.552\%$ ) are sufficiently low, as does a comparison between the refined and the experimental patterns, indicating the high quality of the fit. The crystalline diffraction pattern of the studied sample 10YDC + (20 %) 150Y:  $\alpha\text{-Al}_2\text{O}_3$ , reveals  $\alpha\text{-Al}_2\text{O}_3$  phase having a trigonal unit cell with lattice parameters  $a = 4.7539(6)\text{ \AA}$  and  $c = 12.9918(9)\text{ \AA}$ , in addition to the phases found in LSCF sample. Fig. 2 shows the observed, calculated and difference profiles resulted from the Rietveld analysis of LSCF and 10YDC + (20 %) 150Y:  $\alpha\text{-Al}_2\text{O}_3$  samples.

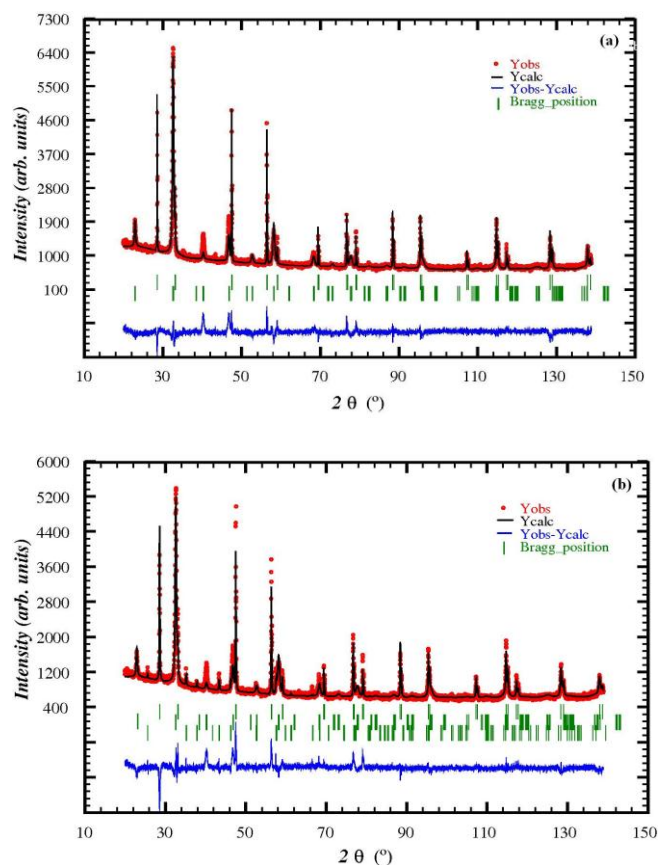


Fig. 2. XRD patterns of (a) LSCF and (b) 10YDC + (20 %) 150Y:  $\alpha\text{-Al}_2\text{O}_3$  samples at RT.

The results obtained by SEM and EDS for the [(80 %) 10YDC + (20%) 150Y:  $\alpha\text{-Al}_2\text{O}_3$ ] sample are shown in Figs. 3 - 4. Fig. 3 shows the agglomerates of 10YDC (used as matrix) and of 150Y:  $\alpha\text{-Al}_2\text{O}_3$  (used as reinforcements). EDS analysis was performed in areas (10YDC  $\rightarrow$  Y-Ce) and (150Y:  $\alpha\text{-Al}_2\text{O}_3$   $\rightarrow$  Y-Al) indicated on Fig. 3. One can observe the low yttria doped alumina agglomerates (2.5 – 8)  $\mu\text{m}$  in diameter, uniformly distributed in the large yttria doped ceria areas. The 10YDC areas consist of spherical agglomerates (1.2 – 4)  $\mu\text{m}$  in size, with an average value of  $(2.22 \pm 0.89)\text{ \mu m}$ . Each spherical agglomerate consists of spherical grains (0.15 – 2)  $\mu\text{m}$ , with an average grain diameter of  $(0.21 \pm 0.072)\text{ \mu m}$  (Fig. 4). In the 150Y:  $\alpha\text{-Al}_2\text{O}_3$  area, one can observe polyhedral grains with an average diameter of  $(1.84 \pm 0.09)\text{ \mu m}$  (Fig. 4). The polyhedral grains of 150Y:  $\alpha\text{-Al}_2\text{O}_3$  have only few intergranular pores. The 10YDC agglomerates have only intergranular pores, especially between the spherical agglomerates. EDS spectra from Fig. 3, evidence only the presence of Ce, Y, O, Ag, and Al, Y, O and Ag elements in (Y-Ce, Y-Al) areas, respectively. We mention that Ag was deposited by evaporation on the sample surface, for metallization purpose.

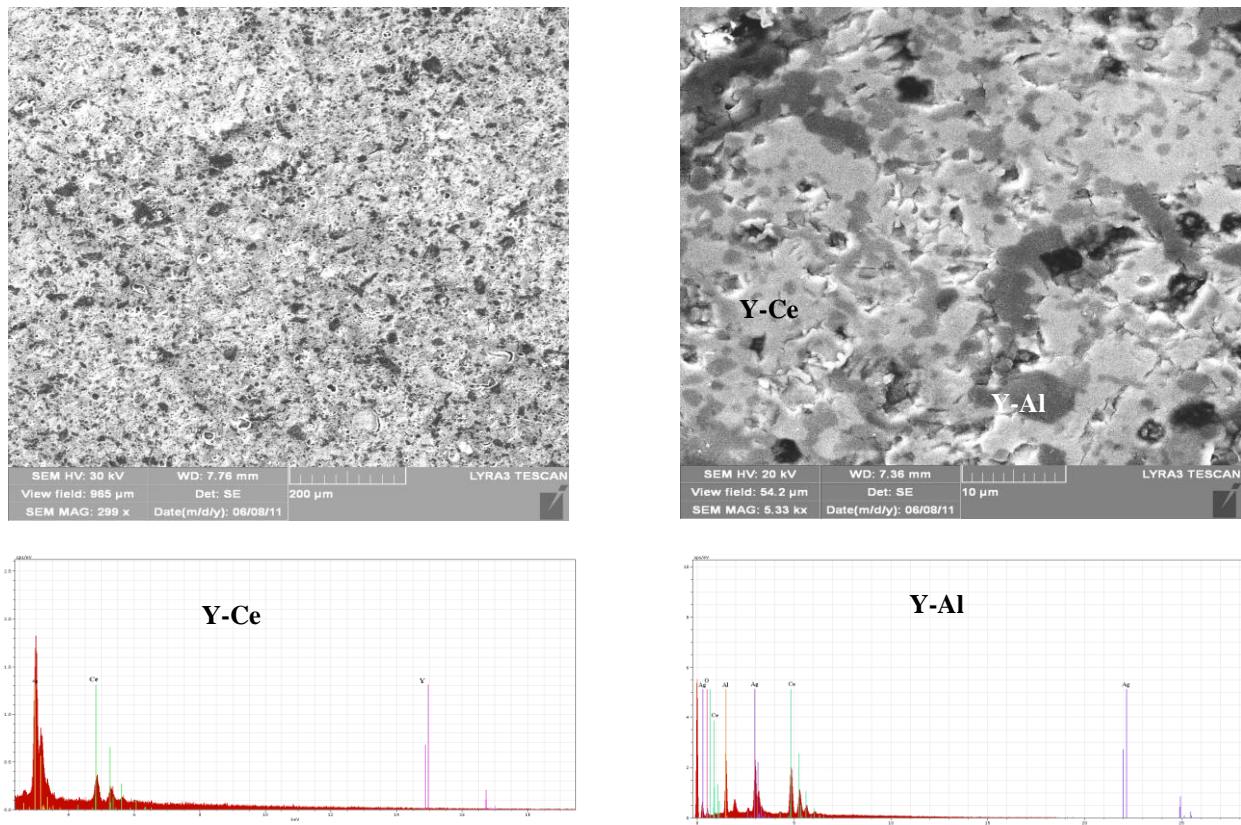


Fig. 3. Typical SEM images and EDS spectra of (80 %) 10YDC + (20%) 150Y:  $\alpha$ -Al<sub>2</sub>O<sub>3</sub>.

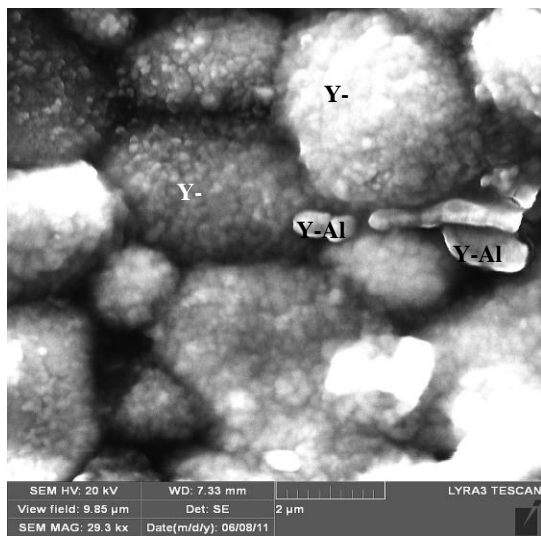


Fig. 4. Typical SEM image of (80%) 10YDC + (20%) 150Y:  $\alpha$ -Al<sub>2</sub>O<sub>3</sub>.

### 3.1.2 Morphological characterization of electrodes

SEM and EDS examination confirmed the presence of electrodes on the electrolyte surface. Fig. 5a shows the cross section of NiO–8YSZ (50:50 vol) on the electrolyte. The grains are irregular and tend to a polyhedral shape with rounded edges. The average diameter of the grains is of  $(6.5 \pm 0.19) \mu\text{m}$ . The inferred porosity was of  $\sim 25\%$ . The EDS spectrum (Fig. 5b) evidences the presence of Ni, Y, Zr, O and Cu elements only.

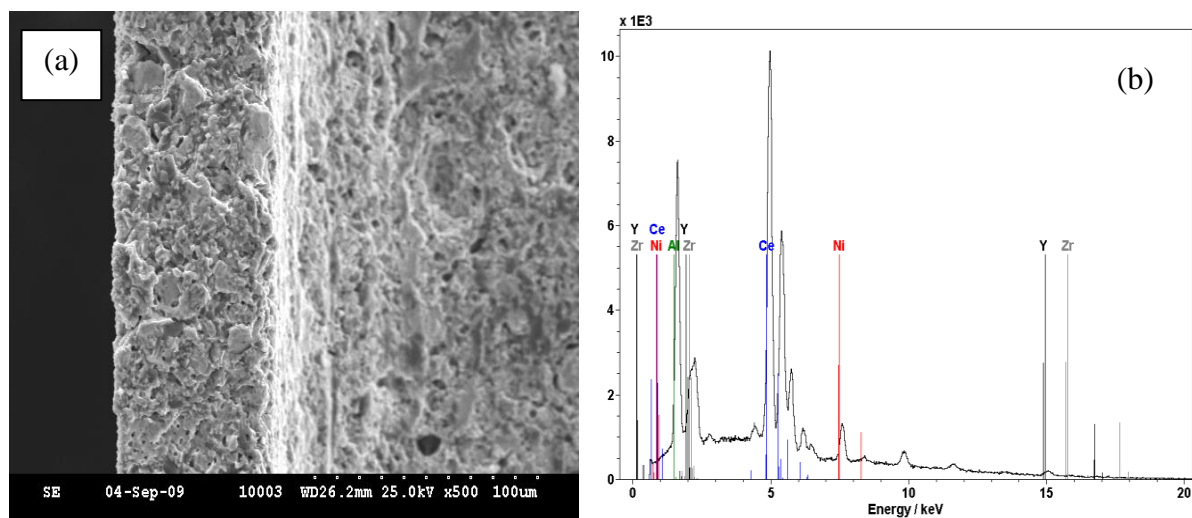


Fig. 5. SEM image (a) and EDS spectrum (b) of anode – cross section.

Fig. 6a shows the cross section of LSCF/ electrolyte. The particles have a polyhedral shape and tend to agglomerate. The average diameter of the grains is of  $(8 \pm 0.19) \mu\text{m}$ . The determined porosity was of  $\sim 32\%$ . The

EDS spectrum (Fig. 6b) shows only the presence of La, Sr, Co, Fe, O and Cu elements.

In case of both electrodes, Cu was deposited by evaporation on the sample surface, for metallization purpose.

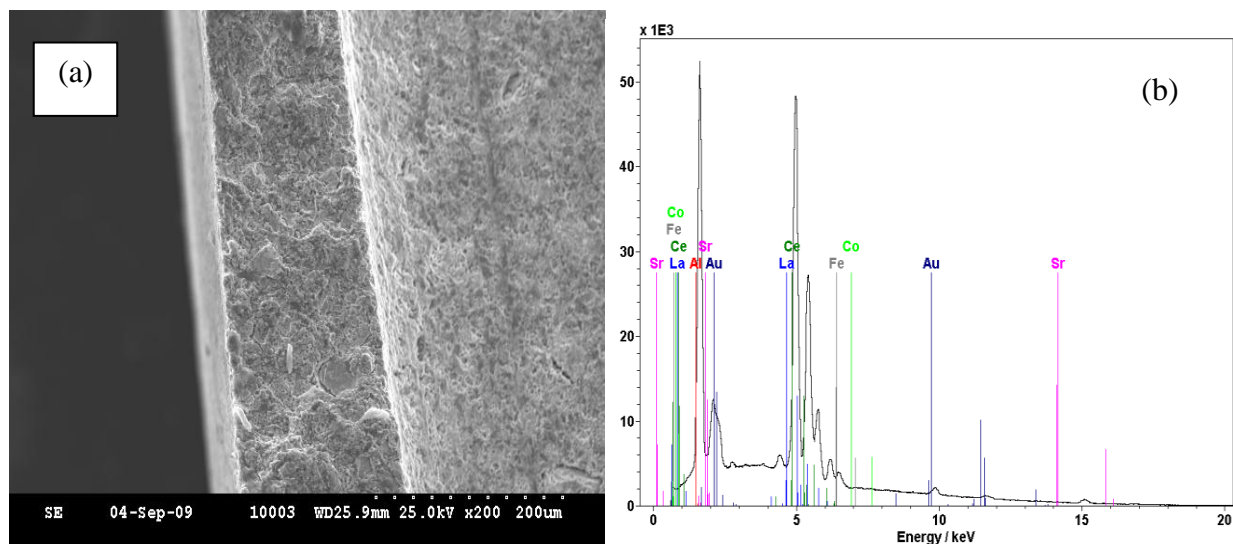


Fig. 6. SEM image (a) and EDS spectrum (b) of cathode – cross section.

### 3.2 Mössbauer spectroscopy

As reported previously [17], X-Ray Diffraction technique proved the crystalline structure of LSCF layers deposited on the electrolyte.

In Fig. 7 the TMS and CEMS spectra of bulk (INFRAMAT, USA) nanopowder and as deposited

cathode layers are plotted. All spectra deposited at RT revealed the coexistence of a central and large resonance line with a sum of sextet-patterns corresponding to the hyperfine magnetic interaction  $^{57}\text{Fe}$  isotope – locale vicinities in the investigated samples.

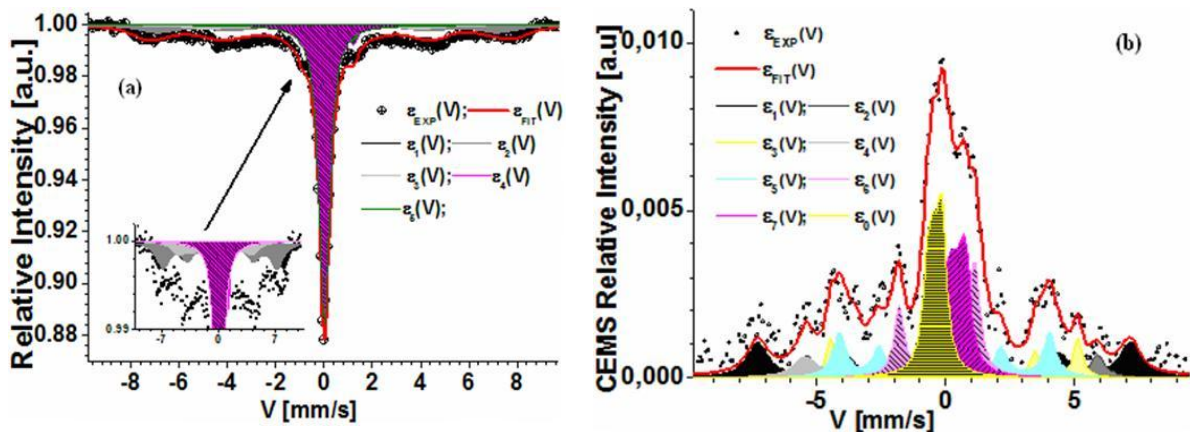


Fig. 7. Mössbauer spectra of cathode recorded at RT: (a) TMS and (b) CEMS geometries.

The hyperfine fit parameters determined for cathode from TMS and CEMS spectra are given in Table 1, for  $^{57}\text{Fe}$  distinct local vicinities of Mössbauer nuclides.

Table 1. The hyperfine fit parameters recorded for cathode from TMS and CEMS spectra.

Patterns	$^a \delta_{S-A}$ [mm/s]	$\epsilon_Q$ [mm/s]	B [T]	$\Gamma_{\text{exp}}$ [m/s]	A [%]
<b>TMS_RT</b>					
1.	0.24	0.035	47.68	1.519	14.52
2.	0.188	-0.015	43.74	2	18.21
3.	0.017	-0.025	0	0.504	51.82
4.	0.35	-0.08	6.65	0.42	6.92
5.	-0.471	0.02	28.14	2	8.55
Errors	$\pm 0.009$	$\pm 0.022$	$\pm 0.5$	$\pm 0.022$	$\pm 3.5$
<b>CEMS_RT</b>					
1.	0.53	-0.09	29.80	0.42	21.24
2.	-0.11	0.04	25.33	0.62	6.91
3.	0.10	-0.07	44.89	1.00	21.50
4.	0.37	-0.05	35.06	0.69	13.87
5.	0.02	-0.18	8.95	0.47	4.16
6.	-0.37	-0.11	0.70	0.43	10.50
7.	0.47	-0.01	2.3	0.47	16.26
8.	1.00	0.12	29.2	1.04	5.56
Errors	$\pm 0.05$	$\pm 0.09$	$\pm 0.68$	$\pm 0.10$	$\pm 5.00$
$^a \delta_{S-A} = ^{57}\text{Co:Rh}$ ; A=LSCF;					

The investigations at RT of cathode powder evidence a magnetic fraction pertaining to a superposition of several sextet patterns and an intense central line. The sextet patterns correspond to the hyperfine magnetic interactions of  $^{57}\text{Fe}$  with its surroundings and are characterized by  $B \in [6.65\text{T} \div 47.68\text{T}]$ , low  $\epsilon_Q$  (around 0), large  $\Gamma_{\text{exp}}$  and

different  $\delta_{S-A}$  values. The low values for  $\epsilon_Q$  points out a high local symmetry around Mössbauer nuclide [18, 19]. Indeed, the arrangement of O ions around metallic cations (B-site) is an octahedral one in perovskite structure, suggesting localized Fe in B-site. Due to the large amount of Fe, the magnetic ordering is expected. The spread of B values and the large  $\Gamma_{\text{exp}}$  values are an indicative of several  $^{57}\text{Fe}$ -surroundings, which are generated by the strontium-doped lanthanum in perovskite structure and/or relaxation phenomena. One knows that the substitution of  $\text{La}^{3+}$  by  $\text{Sr}^{2+}$  produces important effects on hyperfine magnetic fields in perovskites lattice [18]. The ferric valence and high spin configuration state are characteristic to sextets 1,  $B_1 \approx 48\text{T}$ ,  $A_1 \approx 15\%$ . The 2<sup>nd</sup> sextet,  $A_2 \approx 18\%$  and slight lower values of  $\delta_{S-A2} (\approx 0.188\text{mm/s})$  and  $B_2 (\approx 44\text{T})$  corresponds to  $\text{Fe}^{4+}$  high spin configuration rather than to  $\text{Fe}^{3+}$  one. The 5<sup>th</sup> sextet shows a weight of  $A_5 = 8.55\%$ ,  $\delta_{S-A5} = -0.471\text{mm/s}$  and a smaller hyperfine magnetic field  $B_5 \approx 29\text{T}$ , which represents  $B_5 = (3/2:5/2) \cdot B_1$  and which typically corresponds to  $\text{Fe}^{5+}$  in high spin configuration  $S=3/2$  in hyperfine magnetic field [19]. The 4<sup>th</sup> sextet has the lowest  $B_4$  ( $\sim 7\text{T}$ ) and  $A_4 \approx 7\%$ , corresponding to ferric state valence very low spin state  $S=1/2$  [16]. That points out a strong reduced field, probably due to surrounding oxygen vacancies and/or to a relaxation process. The central line  $\delta_{S-A3} \approx 0\text{mm/s}$  is the RT paramagnetic phase. This has the highest weight  $A_3 \approx 52\%$ , and corresponds to  $\text{Fe}^{3+}$  [16].

Both type of spectra show the coexistence of the similar paramagnetic fraction with the magnetic one (patterns 1, 2, 3, 4, 5, 8), but the weight ratio is favourable to the last one ( $\sim 27\%/73\%$ ). The values of magnetic field intensities spread in the same range as observed for TMS spectra recorded at RT. The low quadruple shift values and range of chemical shift have shown that local structure around  $^{57}\text{Fe}$ -nuclide, valence and spin states are similar to both LSCF powder and deposited thin films. For CEMS spectra recorded at RT, the most evidenced patterns were the magnetic ones, with different  $\delta_{S-A}$  and B-values, pointing out the slightly different weights of iron ionic

states. One could notice that not only the patterns of  $\text{Fe}^{3+}$ ,  $\text{Fe}^{4+}$  and  $\text{Fe}^{5+}$  valence states (pattern 2, 3, and 4), but also the  $\text{Fe}^{2+}$  states (patterns 1 and 8) were retrieved. The 5<sup>th</sup> pattern could correspond to  $\text{Fe}^{3+}$  very low spin configuration.

The evidence of similar line-shape of TMS and CEMS spectra recorded at RT (paramagnetic and magnetic fractions, same B-values range, large  $\Gamma_{\text{exp}}$ , and similar iron states), the presence of mixed iron valence and spin states and their dynamics constitute an argument that local structure of Mössbauer nuclide in LSCF deposited layers is the same as in the case of powder.

#### 4. Conclusions

We synthesized by Pulsed Laser Deposition anode (Nickel Oxide-8Yttria Stabilized Zirconia 50:50 vol) and cathode ( $\text{La}_{0.6}\text{Sr}_{0.4}\text{Co}_{0.2}\text{Fe}_{0.8}\text{O}_{3-\delta}$ ) layers. The deposited structures were adherent on the new ceramic composite substrate, [(80%) 10Yttria doped Ceria + (20%) (150Yttria doped  $\alpha$ -Alumina)] used as electrolyte for Intermediate Temperature Solid Oxide Fuel Cells applications. An oxygen flux of  $2 \times 10^{-1}$  Torr, a  $\sim 2.2 \text{ J/cm}^2$  fluence and  $300^\circ\text{C}$  (Nickel Oxide-8Yttria Stabilized Zirconia 50:50 vol) and  $400^\circ\text{C}$  ( $\text{La}_{0.6}\text{Sr}_{0.4}\text{Co}_{0.2}\text{Fe}_{0.8}\text{O}_{3-\delta}$ ) deposition temperatures, made possible to grow layers with an adequate morphology (concerning the porosity, adhesion and the average grain size).

The electrolyte used in the experiments, [(80%) 10Yttria doped Ceria + (20%) (150Yttria doped  $\alpha$ -Alumina)], is considered to be a new material because usual pure  $\alpha$ -Alumina was replaced with (150 Yttria doped  $\alpha$ -Alumina) like reinforcement in the matrix (10Yttria doped Ceria). The electrolyte (sintering bodies obtained at  $1500^\circ\text{C}$ , 2 hours) is a composite in which, the reinforcement (doped alumina) is uniform distributed in the matrix (doped ceria), a very important goal in order to achieve competitive material properties.

Pulsed Laser Deposition is usually applied to deposit thin, high-quality, oriented layers on a single crystal substrate. In these experiments, Pulsed Laser Deposition parameters were set for an unusually fast deposition rate so that micrometer thickness layers could be grown.

Scanning Electron Microscopy correlated with Energy Dispersive X-ray Spectroscopy analysis of the electrolyte clearly confirmed the uniform distribution of the 150Yttria doped  $\alpha$ -Alumina (used as reinforcement) in 10Yttria doped Ceria (used as matrix). Two different areas were obtained: a light area of Yttria doped Ceria with uniform spherical agglomerates/grains and a dark area of Yttria doped Alumina with polyhedral grains with round edges. Energy Dispersive X-ray Spectroscopy of electrodes showed only the presence of constitutive elements of anode and cathode. No impurities were detected.

In this paper, the anode and cathode layers deposited on the electrolyte by laser ablation had a uniform thickness of  $\sim 80$  ( $30 - 40$ )  $\mu\text{m}$  and  $\sim 140$  ( $35-55$ )  $\mu\text{m}$ , respectively.

The anode and cathode layers were porous and the grains were irregular and tend to a polyhedral shape with rounded edges. The obtained values of porosity ( $\sim 25\%$  for anode and  $\sim 32\%$  for cathode) are adequate for fuel supply in Intermediate Temperature Solid Oxide Fuel Cells.

The larger dispersion of all observed parameters in CEMS spectra, but around TMS values, could be explained by the relaxation dynamics. The lines shape similarity in CEMS and TMS spectra is not a surprise taking into account the possibility given by PLD to insure the stoichiometric transfer of oxides from target to collector [10, 21].

The comparison between the fit hyperfine parameters recorded from TMS and CEMS spectra demonstrated that  $^{57}\text{Fe}$  had the same local structure, mixed iron valence and spin states with their dynamics present in bulk and in PLD deposited cathode layers, proving the possibility to use this procedure for LSCF deposited on electrolyte.

Our results conclude that the Pulsed Laser Deposition technique can be used as a suitable method for obtaining electrodes for Intermediate Temperature Solid Oxide Fuel Cells applications.

#### Acknowledgements

The authors are grateful for the support of this research by the Contract NANOCOMSIT 71-031/2007.

#### References

- [1] C. D. Baertsch, K. F. Jensen, J. L. Hertz, H. L. Tuller, S. T. Vengallatore, S. M. Spearing, M. A. Schmidt, J. Mater. Res. **19**, 2604 (2004).
- [2] A. M. Vlaicu, I. Mercioniu, B. S. Vasile, C. C. Negrila, C. Logofatu, N. C. Cretu, P. Nita, N. P. Pogrion, Optoelectron. Adv. Mater. – Rapid Commun. **5**(2), 143 (2011).
- [3] A. M. Ionascu, I. Mercioniu, P. V. Notingher, N. Popescu-Pogrion, Optoelectron. Adv. Mater. – Rapid Commun. **5**(7), 773 (2011).
- [4] I. Mercioniu, U. P. B. Sci. Bull., Series B, **72**(4), (2010).
- [5] H. S. Spacil, US Patent 3,558,360; filed October 30, 1964, modified November 2, 1967, granted March 31, 1970.
- [6] S. C. Singhal, K. Kendall, High Temperature Solid Oxide Fuel Cells: Fundamentals, Design and Applications, Elsevier Advanced Technology, Oxford, UK, 2003.
- [7] N. P. Pogrion, I. Mercioniu, S. Constantinescu, Proceedings Materials Science & Technology Conference MS&T, Detroit, p. 321, 2007.
- [8] S. R. Hui, D. Yang, Z. Wang, S. Yick, C. D. Petit, W. Qu, A. Tuck, R. Maric, D. Ghosh, J. Power Sources **167**, 336 (2007).

- [9] H. J. Cho, G. M. Choi, *Solid State Ionics* **180**, 792 (2009).
- [10] L. Duta, A. C. Popescu, G. Dorcioman, I. N. Mihailescu, G. E. Stan, I. Zgura, I. Enculescu, I. Dumitrescu, chapter 20 in A. Vaseashta, E. Braman, P. Susmann (Eds.) "Technological Innovations in Sensing and Detection of Chemical, Biological, Radiological, Nuclear Threats and Ecological Terrorism", NATO Science for Peace and Security Series A: Chemistry and Biology, Part 4, pp. 207-210, DOI: 10.1007/978-94-007-2488-4\_20, 2012.
- [11] G. Socol, A. C. Galca, C. R. Luculescu, A. Stanculescu, M. Socol, N. Stefan, E. Axente, L. Duta, C. M. Mihailescu, V. Craciun, D. Craciun, V. Sava, I. N. Mihailescu, *Digest Journal of Nanomaterials and Biostructures*, **6**(1), 107 (2011).
- [12] A. C. Popescu, L. Duta, G. Dorcioman, I. N. Mihailescu, G. E. Stan, I. Pasuk, I. Zgura, T. Beica, I. Enculescu, A. Ianculescu, I. Dumitrescu, *J. Appl. Phys.*, **110**(6), 064321, doi:10.1063/1.3639297.
- [13] D. Beckel, U. P. Muecke, T. Gyger, G. Florey, A. Infortuna, L. J. Gauckler, *Solid State Ionics* **178**, 407 (2007).
- [14] H. S. Noh, J. S. Park, J. W. Son, H. Lee, J. H. Lee, H. W. Lee, *J. Am. Ceram. Soc.*, **92**, 3059 (2009).
- [15] A. G. Maddock, *Horwood Chemical Science Series*, Horwood, 1997.
- [16] D. Barb, Ed. *Academiei Romane Bucuresti & Akademie-Verlag Berlin*, 1980.
- [17] I. Mercioniu, N. Cretu, S. Constantinescu, N. P. Pogrion, *Optoelectron. Adv. Mater. – Rapid Commun.*, in press, 2011.
- [18] N. N. Greenwood, T. C. Gibb, *Chapman and Hall*, 1971.
- [19] J. Marzec, *J. Power Sources*, **173**, 671 (2007).
- [20] F. Salvat, J. Parellada, *Phys. Res. B* **1**, 70 (1984).
- [21] I. Fasaki, A. Giannoudakos, M. Stamataki, M. Kompitsas, E. György, I. N. Mihailescu, F. R. Kalantzopoulou, A. Lagoyannis, S. Harissopoulos, *Appl. Phys. A* **91**, 487 (2008).

---

\*Corresponding author: liviu.duta@inflpr.ro